Dynamic structural colour using vanadium dioxide thin films

K. Wilson,[1)] C. A. Marocico,[1)] and A. L. Bradley[1)*]

[1]*School of Physics and CRANN, Trinity College Dublin, Dublin 2, Ireland*

[*]*bradlel@tcd.ie*

Abstract: A thin film stack consisting of layers of Indium Tin Oxide (ITO) with an intermediate Vanadium Oxide (VO_2) layer on an optically thick silver film has been investigated for dynamic structural colour. The structure benefits from the phase change properties of VO_2. Compared with other phase change materials, such as Germanium Antimony Telluride (GST), VO_2 can be offered as a lower power consumption alternative. It has been overlooked in the visible spectral range due to its smaller refractive index change below 700 nm. We demonstrate that the sensitivity of the visible reflectance spectrum to the change in phase of a 30 nm VO_2 layer is increased after it is incorporated in a thin film stack, with performance comparable to other phase change materials. The extent to which dynamic tuning of the reflectance spectra of ITO-VO_2-ITO-Ag thin film stacks can be exploited for colour switching is reported, with approximately 25% change in reflectance demonstrated at 550 nm. Inclusion of a top ITO layer is also shown to improve the chromaticity change on phase transition.

I. INTRODUCTION

Thin film structures are applied across the field of optics for anti-reflection coatings, high reflection mirrors and optical filters. These structures can be as simple a couple of layers of different materials or complex multi-layer aperiodic stacks. There are many examples of thin film structures producing vibrant structural colour across the visible wavelength range[1]. These structures exploit the interference of electromagnetic waves reflected at the interfaces. The

conditions for constructive or destructive interference at each wavelength depend on the phase change on reflection at each interface and the optical thickness of each layer, *nd*, where *n* is the refractive index and *d* is the layer thickness. Traditionally, structures have been fabricated using low absorption dielectric layers so that light can experience multiple passes through complex thin film stacks to exploit most the interference effects. Designs for high reflectance structures often incorporate a back metallic film. More recently, very simple structures formed using a few nanometre thick highly absorbing layer of Ge deposited on an optically thick Au layer have been considered for coloured optical coatings[2]. It was shown that for a sufficiently thin Ge film interference effects could persist, and the desired reflected colour can be selected by varying the thickness of the ultrathin Ge layer.

The ability to electrically tune the response of a thin film stack is of interest for a wide range of applications such as dynamic optical components and colour tuning for displays. This has driven interest in the incorporation of phase change materials (PCMs) within thin film stacks, and dynamic spectral tuning of the reflectance or transmittance has been demonstrated[3,4]. The complex refractive index of PCMs is modified as it transitions from one phase state to another[5-8]. Chalcogenide-based PCMs such as GeSbTe (GST)[8-10] and AgInSbTe (AIST)[11-14] have been previously explored for colour switching devices[15,16], and phase change memory cells for computing[10,11,17]. PCMs have also been widely used in re-writable optical disks such as the DVD format[17,18]. For colour generation, few nanometre thick layers of AIST or GST layer have been sandwiched between two layers of indium tin oxide (ITO), with bi-stable colour switching in the visible wavelength range demonstrated as the material changes from the amorphous to crystalline state [15,16,19-21]. GST also exhibits electrically triggered switching rates on the order of nanoseconds[15]. While these materials offer many advantages, they pose toxicity concerns[22]

and, due to their high absorption, very thin layers are required. For example, in the case of GST layers as thin as 7 nm are required introducing, difficulties for the uniform fabrication of such ultra-thin layers[15].

VO_2 is another PCM which can be considered. VO_2 transitions from a low temperature semiconducting monoclinic phase to a high temperature rutile metallic phase at 68ºC[23], significantly lower than the 170ºC and 145ºC required for AIST[3] and GST[10], respectively. This phase transition can be achieved by heating[5] or it can be electrically triggered[8] with lower power consumption than for AIST or GST. Studies of the mechanism of electrically switching of the VO_2 phase[24-26], show typical threshold electric field magnitudes of the order of 10^7 V/m[25,27]. Steady state switching has been demonstrated with an applied DC voltage[28]. Furthermore, its lower absorption allows for thicker layers, overcoming one of the fabrication difficulties associated with ultra-thin GST layers[15]. VO_2 can be deposited using a wide range of techniques including, but not limited to, sputtering, molecular beam epitaxy and plasma laser deposition. In summary, VO_2 can potentially offer lower toxicity[22], less stringent fabrication constraints[15] and lower power consumption[23], while providing stable, reversible and electrically activated tuning[29].

The refractive index change of VO_2 is greatest in the infra-red and microwave spectral ranges, which has motivated extensive studies using VO_2 for applications in IR waveguides[28,30-31], optical communications[29,32,33], IR sensing[34,35], and many THz applications[30,36,37]. It has also been widely studied for thermochromic windows[38] and, more recently, has been attracting renewed interest for tunable metasurfaces in the IR[39-41]. An ultra-thin layer of VO_2 on a sapphire substrate has been used to demonstrate a thermally tunable perfect absorber in the

IR[42]. The material exhibits a smaller but still significant complex refractive index change in the range below 700 nm[23]. The phase transition produces a maximum change of 60% in n and of 20% in k across the visible spectral range. While, this is lower than that of other PCMs, such as GST with a maximum change of 100% in n and 250% in k over the same spectral range, the advantages of VO_2 described above warrant consideration of its potential for applications in the visible wavelength region. A previous study of VO_2 layers of varying thickness deposited on quartz showed that in the visible region the transmittance of the semiconductor phase is generally lower than that of the metallic phase for film thicknesses less than 35 nm but for thicker films the transmittance of the insulating phase is greater, arising from interference effects[43]. In this paper, we show that the sensitivity to the refractive index change in a VO_2 layer over the visible range can be increased by using multilayer structures comprised of ITO and VO_2 layers on a Ag back-reflector. The extent to which the tuning of the reflectance spectra can be exploited for colour switching is investigated.

II. RESULTS & DISCUSSION

Simulations are carried out using a transfer matrix method (TMM). All data presented in the manuscript is obtained from the numerical simulations. Complex refractive index data for VO_2 has been obtained from Cormier *et al.*[23], for ITO from reference 44, and for Ag and Si from reference 45. ITO is a commonly used transparent conductive oxide[46,47] that can act as the contact material in electrically activated thin film PCM structures[15]. With low absorption, k, and a relatively constant n across the visible, it is suitable for thin film interference structures and for maximising the light interaction with the VO_2 layer. The spectral dependences of n and k for both VO_2 and ITO are shown in Figs. 1(a) and (b), respectively. The reflective structures incorporate an optically thick layer of Ag (100 nm) on a Si substrate which provides high reflectance (>95%)

across the visible spectral range. The Ag layer also exhibits high conductance and can be used as a bottom contact. Ag is often difficult to incorporate into structures due to tarnishing, but in this case, it is sealed from the atmosphere at the bottom of the structure. Si is selected as it is considered a typical substrate, compatible with silicon technology. Other substrates can be used if desired as the substrate does not play an optical role due to the thickness of the Ag layer in this reflective structure. Also shown in Figs. 1(a) and (b) are the *n* and *k* values for both the semiconducting monoclinic (cold) and metallic rutile (hot) states of VO_2. Both *n* and *k* change in the visible range on transition from the semiconducting to the metallic phase. The electrically triggered semiconductor to metal transition has been reported to occur on a timescale within 2 ns, with an on/off resistance ratio of ~100 [25]. Threshold electric field magnitude of the order of 10^7 V/m have also been reported[28]. Electrically actuated switching is preferable to thermal switching for device implementation and relatively fast response times with low power consumption are also advantageous. For a device with a VO_2 thickness of 30 nm, in the configuration shown in Fig. 2 (d), a threshold voltage of 0.54 V would be required. Similar thin film structures, using a 7 nm thick layer of GST have reported threshold voltages of 2.2 V[15]. The thickness dependence of the threshold voltage and power consumption is further discussed later.

Reflectance spectra are calculated for a range of structures and, subsequently, a colour conversion script is used to convert the spectra to a standard red, green and blue (sRGB) colour gamut. The reflectance spectra throughout the manuscript are presented in their corresponding sRGB value colour, unless otherwise stated. The sRGB colour model is a widely used additive model using three primary colours (red, green and blue) in a set of three 8-bit numbers ranging from 0-255. This colour model is often used in digital display technology as pixels used in computer displays are, in the vast majority of cases, made up of three sub-pixels, each of which is

responsible for displaying one of the three primary colours, with the spectral intensity distribution for each colour significantly overlapping with the wavelengths ranges of the three colour cones in the retina of the human eye. The colour conversion process takes the spectrum of a solar source and weights it separately against three integral functions, one for each of the primary colour cone photoreceptors. Equal area integrals are used, rather than specifying luminance for each cone. The normalised integrated colour matching functions are then weighted according to their relative cone sensitivity to produce the final colour matching functions, presented as an 8-bit number, ranging from 0-255. sRGB values combine luminance and chromaticity of a colour.

Luminance is a measure of luminous spectral intensity, and in colour vision indicates how much luminous power will be detected by an observer of an object or surface from a particular angle of observation. The larger the luminance value of the colour, the higher the visibility of that colour under the observation conditions. Chromaticity is an objective quantitative measure of the quality of colour, and is independent of the luminance value of the object or surface being observed. Chromaticity values represent all discernible different colours that can be perceived by humans using the three colour cones in the retina. For example, a sRGB of 255:4:4 indicates a predominantly red colour of maximum luminance, and so would be visible as a bright, pure red colour to the human eye. A value of 63:1:1 also represents a red colour of the same chromaticity (as the relative weighting is the same) but at a quarter of the luminance, and so would be visible as a darker red colour. With over 16 million different combinations available using this method, it can be used to comprehensively represent the full range of human colour vision.

The Commission Internationale de L'Eclairage (CIE) colour-map is used later in Fig. 4 to determine trends and qualitatively analyze colour clarity. The centre point represents the area of

lowest colour clarity, and indicates a spectrum that has equal stimulation of all three colour cone regions. Moving out from this centre point towards the border of the sRGB region improves colour clarity. The red, green and blue primaries represent the positions on the CIE colour-map that have the highest colour clarity. In order for a colour to be positioned in close proximity to one of these positions, it must have a substantial reflectance intensity in only one of the three colour cone regions of the visible spectrum, while having significantly smaller reflectance in the other two.

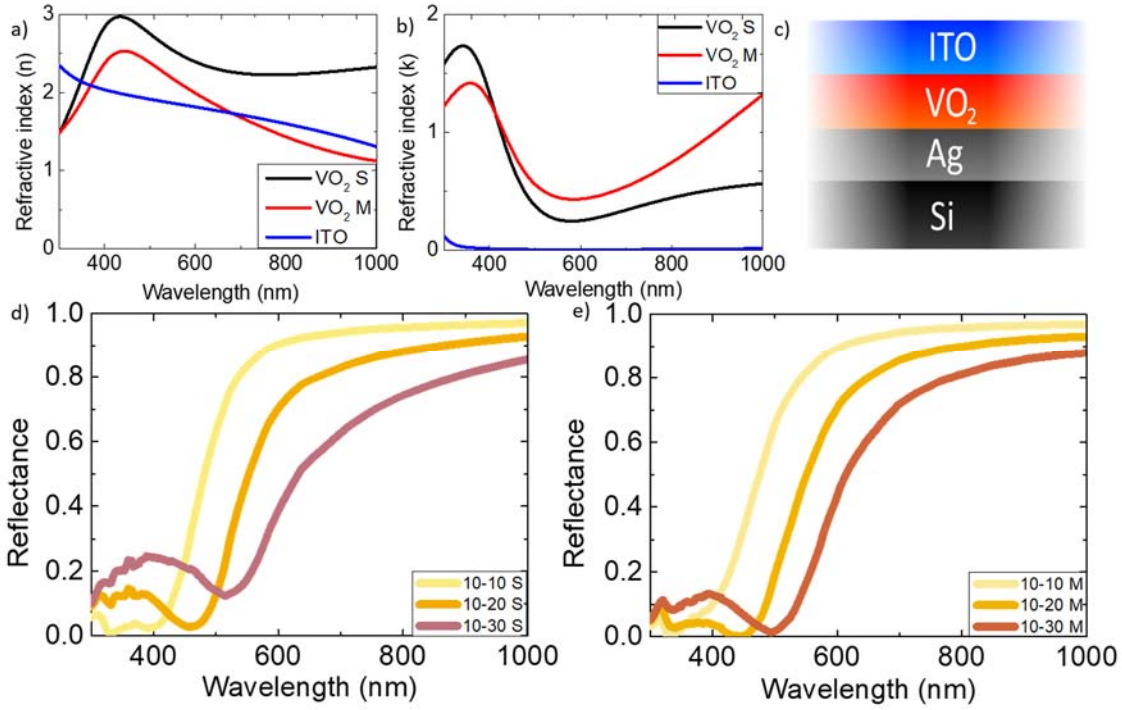

Fig. 1. (a) Real component of the refractive index (*n*) of monoclinic semiconducting (cold) phase and rutile metallic (hot) phase of VO_2, and of ITO material used as transparent contact. (b) Imaginary component of the refractive index (*k*). (c) Schematic of the three-layer thin film structure consisting of ITO as a transparent contact, VO_2 as a phase change material, silver as a back-reflector and second contact, on a silicon substrate. (d) and (e) Reflectance spectra of three structures consisting of 10 nm of ITO, and varying VO_2 thickness of 10 nm, 20 nm and 30 nm in the semiconducting (S) and metallic (M) phases. The line for each spectrum is shown in the sRGB value colour.

Firstly, we introduce the simplest three-layer structure consisting of ITO, VO_2 and Ag on a Si substrate, shown in Fig. 1(c). The reflectance spectra for this structure with semiconducting and metallic phases of VO_2 are shown in Figs. 1(d) and 1(e), respectively. VO_2 layer thicknesses of 10 nm, 20 nm and 30 nm are considered with a fixed 10 nm thick top ITO layer. The visible colour in reflection varies from yellow toward red as the VO_2 thickness increases. The change in colour is predominantly due to the increased absorption with thicker VO_2 layers. Only limited spectral changes are evident after the phase transition, with a maximum ΔR value of 16% at 465 nm observed for the 30 nm VO_2 structure. The change in k and, consequently, the size of the change in reflectance, $\Delta R = R_S - R_M$, induced by the phase transition is low, where R_S and R_M are the reflectance of the semiconductor and metallic phase structures, respectively. For thicker VO_2 layers, absorption is increased, resulting in lower reflectivity across the visible region. As a result, any changes in spectral shape will be less evident for thicker layers, as the low reflectivity will produce colours with low luminance which are hard to distinguish from each other. Such a simple structure does not allow for full exploitation of thin film interference effects.

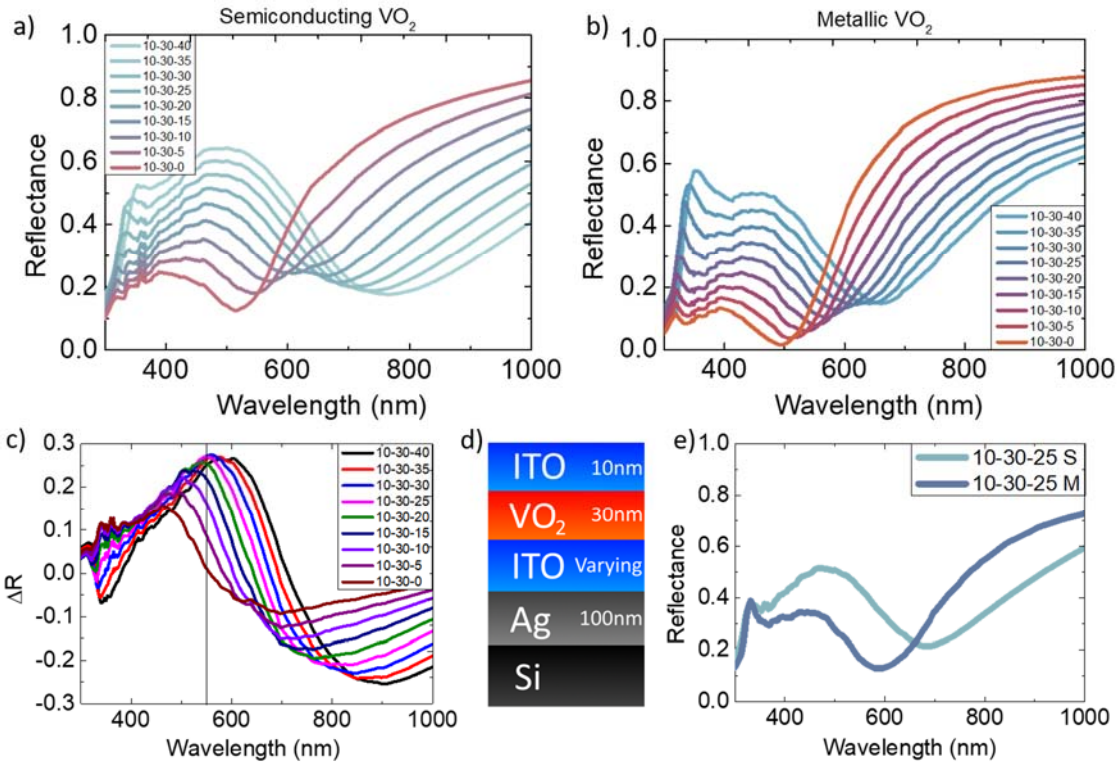

Fig. 2. (a) and (b) Reflectance spectra for the structure shown in (d) for VO_2 in the semiconducting phase and metallic phase, respectively, for varying thickness of the bottom ITO layer from 0 nm to 40 nm. (c) ΔR ($=R_S$-R_M) spectral dependence, where R_S is the reflectance for the semiconducting phase and R_M is the reflectance for the metallic phase. (e) The reflectance spectra for the structure showing the largest ΔR after the transition from the semiconducting to metallic phase.

The change in complex refractive index of the VO_2 PCM layer can be better exploited when is sandwiched between ITO layers on top of the Ag back reflector, as shown in Fig. 2(d). The thickness of the top ITO layer is fixed at 10 nm and that of the VO_2 layer at 30 nm. The thickness of the bottom ITO layer is varied from 0 nm to 40 nm. The reflectance spectra for the semiconducting and metallic phases are shown in Figs. 2(a) and 2(b), respectively. Firstly, the colour tuning as a function of the ITO layer thickness can be observed. For VO_2 in the semiconducting phase, Fig. 2(a), the peak at approximately 400 nm and the dip in reflectance at 500 nm redshift as the ITO layer thickness increases. The redshift of the dip is almost twice that

of the peak, which causes a broadening of the spectral feature, and the peak reflectance values increase as the ITO thickness increases. The higher reflectance at longer wavelengths shifts towards the IR, causing a reduction in the stimulation of red cone receptors. Reflectance intensity across the green and blue cones increases as thickness increases and due to the increase in the width of spectral features, there is an overall reduction in colour clarity. There is also an increase in luminance, as the peak reflectance is higher. This indicates that using thinner layers of ITO produces structures with better chromaticity due to narrower spectral features, a point that is discussed further in Fig. 4. Comparing the semiconducting phase with the metallic phase, it can be seen that the redshift of the spectral features is much larger for the semiconducting phase, and higher minimum reflectance results in lower luminance (colour clarity) than for the metallic phase. Figure. 2(c) clearly demonstrates that the introduction of the bottom ITO layer provides for much larger changes in reflectance, ΔR, reaching values of over 25% for a bottom ITO layer greater than 25 nm thick. This can be compared with 15% in the absence of the bottom ITO layer for the same thickness of VO_2. The peak position of ΔR redshifts by approximately 15 nm for each 5 nm increase in ITO thickness. The cavity structure has greatly increased the sensitivity of the visible reflectance spectra to the phase of the VO_2 layer. These ΔR values are similar to those reported in the literature for GST and AIST structures[15][16].

However, structures exhibiting the greatest ΔR values do not necessarily lead to significant changes in colour. For example, the spectra in Fig. 2(e) correspond to the largest ΔR observed at 550nm, the centre of the visible region. The structure has a 10 nm top ITO layer, 30 nm VO_2 layer and 25 nm bottom ITO layer. In the semiconducting phase a rather broad intense spectral feature overlaps with three colour cones, and in particular with the blue and green cones. In the metallic phase, there is a reduction in luminance across the visible region, with a markedly lower minimum

reflectance at the dip at 580 nm. This causes a reduction in stimulation of the red colour cone and a shift in chromaticity is towards the blue primary. While ΔR is a measure of the sensitivity of the reflectance of a structure to the phase change material, its use is limited for determining structures for optimal spectral tuning. It does not differentiate between changes in the reflectance values and spectral shifts, where the former has a stronger impact on luminance and the latter on chromaticity.

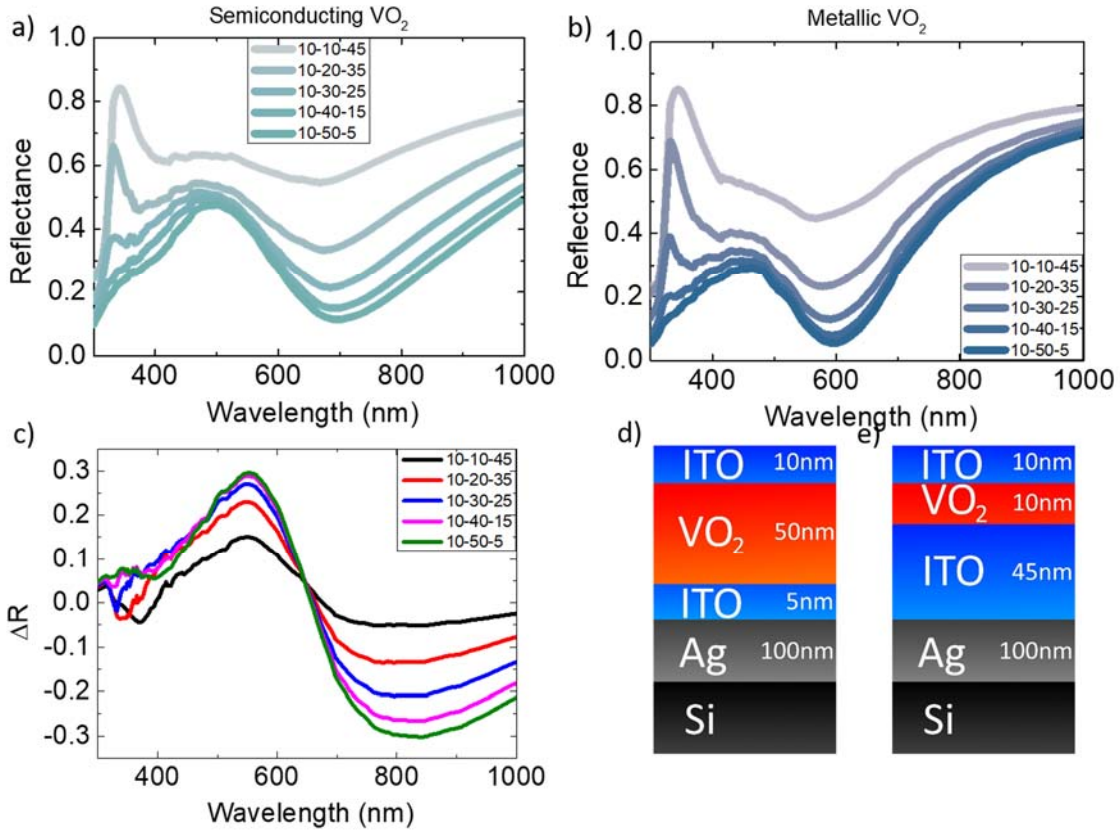

Fig. 3. (a) and (b) Reflectance spectra of ITO/VO_2/ITO/Ag/Si stack structure with total VO_2 layer and bottom ITO layer thickness of 55 nm with varying thickness of VO_2 from 10-50nm in 10nm steps, for the semiconducting and metallic phase, respectively. (c) ΔR values for phase change of the material, showing a maximum ΔR for this stack configuration at 30% at 550nm. (d) and (e) Schematics showing the structures for the thickest VO_2 (d) and ITO (e) layers.

To further optimise the ITO cavity structure we look at the impact of the thickness of the VO_2 layer, where the combined thickness of the VO_2 layer and bottom ITO layer is kept constant at 55 nm, see Figs. 3(d) and 3(e). In this way, the spectral peaks and troughs are maintained at approximately the same positions while the VO_2 thickness changes. The spectra for the semiconducting and metallic phases are shown in Figs. 3(a) and 3(b), respectively. The ΔR values shown in Fig. 3(c) are now independent of any spectral shifts and can be used to identify the structure that has the greatest sensitivity to the phase change of the VO_2 layer. As expected increasing the thickness of the absorbing VO_2 layer results in an increase in absorption and reduced luminance. The difference in reflectance values at the peak and trough increases with increasing VO_2 thickness, with spectral features becoming more defined. This leads to a reduction in the simultaneous stimulation of multiple colour cones, producing a trend away from pastel colours to values closer to the red, green, and blue primaries. Little change in the colour produced for each phase or the ΔR values across the visible part of the spectrum is observed for thicknesses greater than 30 nm, with a maximum ΔR of approximately 30% at 550 nm. It can be noted that if the bottom ITO layer thickness is fixed at 25 nm then the positions of the peaks will also shift as the VO_2 thickness is increased, however there is no effect on the maximum ΔR value obtained on phase transition (data not shown).

The threshold voltage and power consumption vary with VO_2 thickness. The power consumption can be minimized by having the device in series with an external resistor, R_{ext}[48]. The power consumption is $P \approx \frac{V_{S\rightarrow M}^2}{R_{ext}}$ where the switching voltage is $V_{S\rightarrow M} = V_{VO_2}\left[1 + \frac{R_{ext}}{R_{VO_2}}\right]$ and R_{VO_2} is the resistance in the semiconducting phase. The power consumption can be minimized by increasing the external voltage but this will cause an increase in the switching voltage. The

optimum corresponds to $R_{ext} \approx R_{VO_2}$ [48]. The power consumption also depends on the pixel size, which is application dependent. Taking an example with a 10 µm x10 µm area pixel, a 30 nm thick VO_2 layer, threshold electric field of 1.8 $\times 10^7$ V/m[28] and ρ ~ 2 Ω.cm[49]. We obtain $R_{VO_2} = \rho \frac{l}{A} = 6\Omega$, a switching voltage $V_{S \to M} = 1.08$ V and power consumption of 194 mW. The switching voltage and power consumption reduce to 0.36 V and 64.8 mW, respectively, for a 10 nm VO_2 layer.

In Fig. 4, the range of colours that can be achieved, the impact of the top ITO contact layer and the change in chromaticity of the reflected colour induced by the semiconductor to metal transition are examined by plotting the sRGB data on a CIE colour-map. Colours of different luminance values but with the same chromaticity are shown at the same position on a CIE colour map.The white in the centre of the colour space is the point at which sRGB values of equal distribution will be located, irrespective of the luminance, while any other mix of these values will be placed within the area bordered by the triangle.

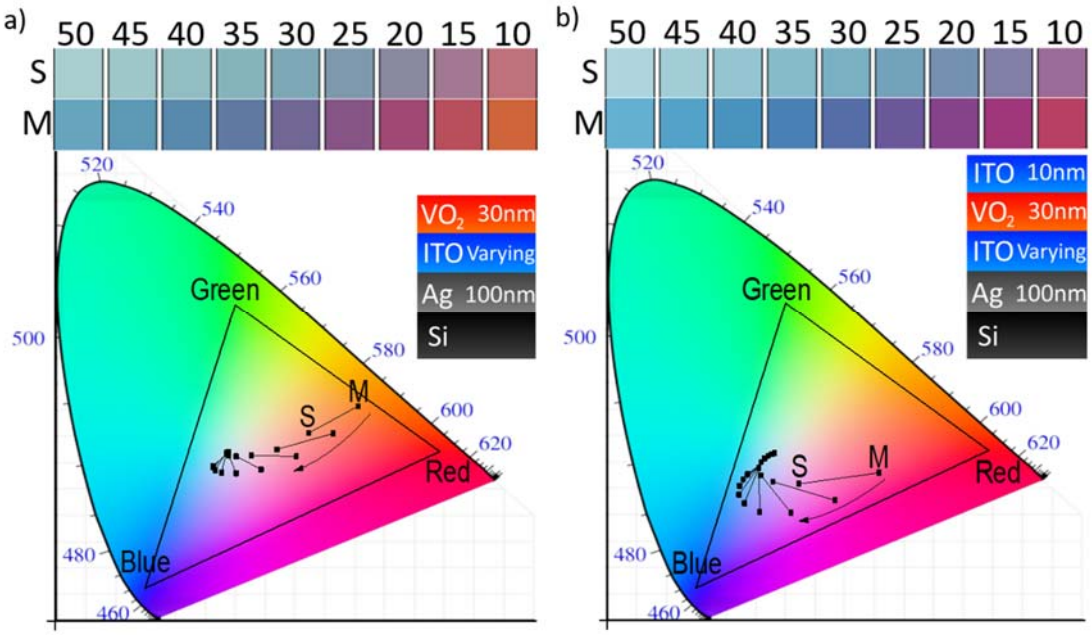

Fig. 4. CIE map (a) with no top ITO layer and (b) with a 10 nm top contact ITO layer. Both cases have a 30 nm thick VO_2 and varying thickness of ITO below the VO_2 layer.

Figure 4(a) shows the data for varying bottom ITO layer thickness and no top ITO layer. For the thinnest ITO layer of 10 nm the CIE colour point, labelled S for the semiconductor phase, the position on the CIE map is near the midpoint of the red and green primaries. After transition to the metal phase the spectral features narrow and reduce in intensity, resulting in a shift towards the border of the sRGB gamut, labelled M. As the ITO layer thickness increases the colour for the semiconducting phase moves closer to the blue primary, and spirals towards the centre. The change in position on the colour-map after the transition to the metallic phase decreases with increasing ITO layer thickness. In all cases the change is towards a more defined single colour, with lower luminance after semiconductor to metal transition. ITO thickness must be kept low in order to maintain chromaticity values closer to the sRGB borders.

Figure 4(b) also shows the colour dependence on the bottom ITO layer thickness in a structure including a top ITO layer. Again, the increasing bottom ITO layer thickness results in a spiraling of the S and M positions towards the centre of the CIE map, and a reduction in the colour change after phase transition. As for the previous structure, there is little change for structures with intermediate ITO layers thicker than 30 nm. The colour positions for the S and M phases for the thinnest ITO layer is closer to the blue primary than in Fig. 4(a). It is noteworthy that the positions for all structures shown in Fig. 4(b) are further from the centre position than those in Fig. 4(a). This is a consequence of the narrower spectral features. The presence of the top ITO layer improves the performance of the structure upon phase transition, as chromaticity changes more significantly. It is of interest to note that, while the 10-30-25 structure demonstrated the largest ΔR value of all structures tested, the CIE plot shows that the 10-30-10 structure demonstrates the most significant

change in chromaticity as seen in the largest movement across the CIE colour-space from one primary to another. This signifies that the ΔR parameter alone does not provide sufficient insight as a method to determine the optimal structure for colour change and utilising the CIE colour map is a more comprehensive method for analyzing the colour tuning properties. Trends are more difficult to follow when chromaticity and luminance values are desired, though luminance values can be shown for each position as a numerical label. It is noted that the range of structures investigated could not provide access to the full CIE colour-space, with the green spectral range in particular unsupported.

II. CONCLUSION

The extent to which the phase change in VO_2 can be exploited for modulated reflectance and colour change in the visible spectral range in a simple planar ITO-VO_2-ITO-Ag structure has been investigated. Incorporation of a thin film of VO_2 in a multilayer stack offers greater change in reflectance and larger spectral tuning than a simpler ITO-VO_2-Ag structure. The intermediate ITO layer plays an important role in fully exploiting thin film interference effects. Structures with 10 nm of ITO under a 30 nm VO_2 layer were found to offer the largest dynamic colour tuning range as the phase state transitions from semiconductor to metal. This structure had the largest movement across the CIE colour-map of any structure examined, though the ΔR value was 22% at 500nm, smaller than the 10-30-25 structure that exhibited a maximum change of 25% at 550nm. The VO_2/ITO structure does not provide access to the full CIE colour-space, with the green spectral range unsupported. Further investigation of nanostructured VO_2-metal structures could extend the colour space. VO_2 has the advantage of lower temperature or voltage requirements for tuning between phase states, and lower absorption than other PCMs allows for finer control of reflectance and colour by layer thickness. However, switching performance, in terms of the change in

reflectance ΔR, is found to be comparable with other PCM-based thin film stacks, with potential for device applications in displays, optical memory switches and dynamic optical components.

ACKNOWLEDGEMENTS

Science Foundation Ireland (SFI) Grant Number SFI/16/IA/4450 and SFI/10/IN.1/12975. KW acknowledges the Irish Research Council, GOIPG/2013/851.

REFERENCES

1. M. A. Kats and F. Capasso, "Optical absorbers based on strong interference in ultra-thin films," Laser Photonics Rev. **10**(5),735–749 (2016).
2. M. A. Kats, R. Blanchard, P. Genevet, and F. Capasso, "Nanometre optical coatings based on strong interference effects in highly absorbing media," Nat. Mater. **12**(1), 20–24 (2012).
3. Y. C. Her, H. Chen, and Y. S. Hsu, "Effects of Ag and In addition on the optical properties and crystallization kinetics of eutectic $Sb_{70}Te_{30}$ phase-change recording film," J. Appl. Phys. **93**(12), 10097–10103 (2003).
4. Y. Ikuma, Y. Shoji, M. Kuwahara, X. Wang, K. Kintaka, and H. Kawashima, "Reversible switching of an optical gate using phase-change material and Si waveguide," OSA Technical Digest (Optical Society of America, 2010), paper IWA6, 5–7(2010).
5. T. Cao, C. Wei, R. E. Simpson, L. Zhang, and M. J. Cryan, "Broadband polarization-independent perfect absorber using a phase-change metamaterial at visible frequencies," Sci. Rep. **4**(1), 3955 (2015).
6. M. Gurvitc, S. Luryi, A. Polyakov, A. Shabalov, M. Dudley, G. Wang, S. Ge, and V. Yakovlev, "VO_2 films with strong semiconductor to metal phase transition prepared by the precursor oxidation process," J. Appl. Phys. **102**(3), 033504(2007).

7. X. Chen, Q. Lv, and X. Yi, “Smart window coating based on nanostructured VO_2 thin film,” Optik (Stuttg). **123**(13), 1187–1189 (2012).
8. M. Rudé, V. Mkhitaryan , A. E. Cetin , T. A. Miller , A. Carrilero , S. Wall , J. García de Abajo , H. Altug, and V. Pruneri, “Ultrafast and broadband tuning of resonant optical nanostructures using phase-change materials,” Adv. Opt. Mater. **4**(7), 1060–1066(2016).
9. J. Orava, A. L. Greer, B. Gholipour, D. W. Hewak, and C. E. Smith, “Characterization of supercooled liquid $Ge_2Sb_2Te_5$ and its crystallization by ultrafast-heating calorimetry,” Nat. Mater. **11**(4), 279–283 (2012).
10. L. Perniola, V. Sousa, A. Fantini, E. Arbaoui, A. Bastard, M. Armand, A. Fargeix, C. Jahan, J. F. Nodin, A. Persico, D. Blachier, A. Toffoli, S. Loubriat, E. Gourvest, G. B. Beneventi, H. Feldis, S. Maitrejean, S. Lhostis, A. Roule, O. Cueto, G. Reimbold, L. Poupinet, T. Billon, B. De Salvo, D. Bensahel, P. Mazoyer, R. Annunziata, P. Zuliani, and F. Boulanger, “Electrical behavior of phase-change memory cells based on GeTe,” IEEE Electron Device Lett. **31**(5), 488–490 (2010).
11. T. Matsunaga, J. Akola, S. Kohara, T. Honma, K. Kobayashi, E. Ikenaga, R. O. Jones, N. Yamada, M. Takata, and R. Kojima, “From local structure to nanosecond recrystallization dynamics in AgInSbTe phase-change materials,” Nat. Mater. **10**(2), 129–134 (2011).
12. T. E. Hsieh Y. J. Huang, T. C. Chung, and C. H. Wang, “Phase transition behaviors of AgInSbTe-SiO_2nanocomposite thin films for phase-change memory applications,” Materials Research Society Proc. **1251**, 55-60 (2010).
13. X. Jiao, J. Wei, F. Gan, and M. Xiao, “Temperature dependence of thermal properties of $Ag_8In_{14}Sb_{55}Te_{23}$ phase-change memory materials,” Appl. Phys. A **94**(3), 627–631 (2009).

14. A. Dun, J. Wei, and F. Gan, “Laser direct writing pattern structures on AgInSbTe phase change thin film,” Chinese Opt. Lett. **9(**8), 8–11 (2011).
15. P. Hosseini, C. D. Wright, and H. Bhaskaran, “An optoelectronic framework enabled by low-dimensional phase-change films,” Nature **511**(7508), 206–211 (2014).
16. C. Ríos, P. Hosseini, R. A. Taylor, and H. Bhaskaran, “Color depth modulation and resolution in phase-change material nanodisplays,” Adv. Mater. **28**(23), 4720–4726 (2016).
17. Y. Lu, S. Song, Y. Gong, Z. Song, F. Rao, L. Wu, B. Liu, and D. Yao, “Ga-Sb-Se material for low-power phase change memory,” Appl. Phys. Lett. **99**(24), 1–4 (2011).
18. C. N. Afonso, J. Solis, and F. Catalina, “Ultrafast reversible phase-change in GeSb films for erasable optical storage,” Appl. Phys. Lett. **60**(25), 3123–3125 (1992).
19. B. Lee, G. W. Burr, R. M. Shelby, S. Raoux, C. T. Rettner, S. N. Bogle, K. Darmawikarta, S. G. Bishop, and J. R. Abelson, “Observation of the role of subcritical nuclei in crystallization of a glassy solid,” Science **326**(5955), 980–984 (2009).
20. D. Shakhvorostov, R. A. Nistor, L. Krusin-Elbaum, G. J. Martyna, D. M. Newns, B. G. Elmegreen, X. Liu, Z. E. Hughes, S. Paul, C. Cabral, S. Raoux, D. B. Shrekenhamer, D. N. Basov, Y. Song, and M. H. Müser, “Evidence for electronic gap-driven metal-semiconductor transition in phase-change materials,” Proc. Natl. Acad. Sci. **106**(27),10907–10911 (2009).
21. Y. Fukuyama, N. Yasuda, J. Kim, H. Murayama, Y. Tanaka, S. Kimura, K. Kato, S. Kohara, Y. Moritomo, T. Matsunaga, R. Kojima, N. Yamada, H. Tanaka, T. Ohshima, and M. Takata, “Time-resolved investigation of nanosecond crystal growth in rapid-phase-change materials: Correlation with the recording speed of digital versatile disc media,” Appl. Phys. Express **1**(4),0450011–0450013 (2008).

22. S. Sundar and J. Chakravarty, “Antimony toxicity,” Int. J. Environ. Res. Public Health **7**(12), 4267–4277 (2010).

23. P. Cormier, T. V. Son, J. Thibodeau, A. Doucet, V. Van Truong, and A. Haché, “Vanadium dioxide as a material to control light polarization in the visible and near infrared,” Opt. Commun. **382**, 80–85(2017).

24. B. G. Chae, H. T. Kim, D. H. Youn, and K. Y. Kang, “Abrupt metal-insulator transition observed in VO_2 thin films induced by a switching voltage pulse,” Physica B: Cond. Matt. **369**(1-4), 76-80 (2005).

25. Y. Zhou, X. Chen, C. Ko, C. Mouli, and S. Ramanathan, “Voltage-triggered ultrafast phase transition in vanadium dioxide switches,” IEEE Elec. Dev. Lett. **34**(2), 220-222 (2013).

26. A. Stabile, S. K. Singh, T. L. Wu, L. Whittaker, S. Banerjee, and G. Sambandamurthy, “Separating electric field and thermal effects across the metal-insulator transition in vanadium oxide nanobeams”, App. Phys. Lett. **107**(1), 013503 (2015).

27. G. Stefanovich, A. Pergament, and D. Stefanovich, “Electrical switching and Mott transition in VO_2,” J. Phys. Cond. Matt. **12**(41), 8837-8845 (2000).

28. P. Markov, R. E. Marvel, H. J. Conley, K. J. Miller, R. F. Haglund, and S. M. Weiss, “Optically monitored electrical switching in VO_2,” ACS Photonics **2**(8), 1175-1182 (2015).

29. A. Crunteanu, M. Fabert, J. Givernaud, V. Kermène, A. Desfarges-Berthelemot, J. C. Orlianges, C. Champeaux, and A. Catherinot, “Vis-IR optical switching/modulation based on the electrically-activated phase transition of VO_2 thin films,” Conference on Lasers and Electro-Optics 2010, OSA Technical Digest (CD) (Optical Society of America, 2010), paper JWA88

30. R. A. Soref, “Phase-change materials for electro-optical switching in the near- and mid-infrared,” Adv. Photonics 2015, paper IW1A.3(2015).
31. S. D. Ha, Y. Zhou, C. J. Fisher, S. Ramanathan, and J. P. Treadway, “Electrical switching dynamics and broadband microwave characteristics of VO_2 radio frequency devices,” J. Appl. Phys. **113**(18), 184501 (2013).
32. S. Chen, X. Yi, H. Ma, H. Wang, X. Tao, M. Chen, and C. Ke, “A novel structural VO_2 micro-optical switch,” Opt. Quantum Electron. **35**(15), 1351–1355 (2003).
33. J. Hiltunen, J. Puustinen, A. Sitomaniemi, S. Pearce, M. Charlton, and J. Lappalainen, “Self-modulation of ultra-fast laser pulses with 1550 nm central wavelength in VO_2 thin films,” Appl. Phys. Lett. **102**(12), 121111 (2013).
34. H. Jerominek, F. Picard, and D. Vincent, “Vanadium oxide films for optical switching and detection,” Opt. Eng. **32**(9),2092 (1993).
35. E. Strelcov, Y. Lilach, and A. Kolmakov, “Gas sensor based on metal-insulator transition in VO_2nanowire thermistor,” Nano Lett. **9**(6),2322–2326 (2009).
36. P. U. Jepsen, B. M. Fischer, A. Thoman, H. Helm, J. Y. Suh, R. Lopez, and R. F. Haglund, Jr, “Metal-insulator phase transition in a VO_2 thin film observed with terahertz spectroscopy,” Phys. Rev. B - Condens. Matter Mater. Phys. **74**(20), 1–9 (2006).
37. T. T. Lv, Y. X. Li, H. F. Ma, Z. Zhu, Z. P. Li, C. Y. Guan, J. H. Shi, H. Zhang, and T. J. Cui, “Hybrid metamaterial switching for manipulating chirality based on VO_2 phase transition,” Sci. Rep. **6**(23186), 1-9(2016).
38. M. Zhou, J. Bao, M. Tao, R. Zhu, Y. Lin, X. Zhang, and Y. Xie, “Periodic porous thermochromic VO_2(M) films with enhanced visible transmittance,” Chem. Commun. **49**(54), 6021 (2013).

39. L. Liu, L. Kang, T. S. Mayer, and D. H. Werner, “Hybrid metamaterials for electrically triggered multifunctional control,” Nat. Commun. **7**, 13236(2016).

40. K. Appavoo and R. F. Haglund, “Detecting nanoscale size dependence in VO_2 phase transition using a split-ring resonator metamaterial,” Nano Lett.**11**(3), 1025–1031 (2011).

41. M. S. Weimer, I. S. Kim, P. Guo, R. D. Schaller, A. B. F. Martinson, and A. S. Hock, “Oxidation state discrimination in the atomic layer deposition of vanadium oxides,” Chem. Mater. **29**(15), 6238–6244 (2017).

42. M. A. Kats, D. Sharma, J. Lin, P. Genevet, R. Blanchard, Z. Yang, M. M. Qazilbash, D. N. Basov, S. Ramanathan, and F. Capasso, “Ultra-thin perfect absorber employing a tunable phase change material,” Appl. Phys. Lett. **101**(22), 221101 (2012).

43. G. Xu, P. Jin, M. Tazawa, and K. Yoshimura, “Tailoring of luminous transmittance upon switching for thermochromic VO_2films by thickness control,” Japanese J. Appl. Physics, Part 1 Regul. Pap. Short Notes Rev. Pap. **43**(1),186–187 (2004).

44. T. A. König, R. A. Ledin, J. Kerszulis, M. A. Mahmoud, M. A. El-sayed, J. R. Reynolds, and V. V. Tsukruk, “Electrically tunable plasmonic behavior of nanocube - polymer nanomaterials induced by a redox-active electrochromic polymer,” ACS Nano **8**(6),6182–6192 (2014).

45. E. D. Palik, *Handbook of Optical Constants of Solids* (Academic, 2012).

46. Y. Leterrier, L. Médico, F. Demarco, J. A. E. Månson, U. Betz, and M. F. Escolà, “Mechanical integrity of transparent conductive oxide films for flexible polymer-based displays,” Thin Solid Films **460**(1-2), 156–166 (2004).

47. H. Hosono, H. Ohta, M. Orita, K. Ueda, and M. Hirano, “Frontier of transparent conductive oxide thin films,” Vacuum **66**(3–4),419–425 (2002).

48. L. Sánchez, A. Rosa, A. Griol, A. Gutierrez, P. Homm, B. Van Bilzen, M. Menghini, J. P. Locquet, and P. Sanchis, “Impact of the external resistance on the switching power consumption in VO_2 nano gap junctions,” App. Phys. Let. **111**(3), 031904 (2017).
49. A. Joushaghani, J. Jeong, S. Paradis, D. Alain, J. S. Aitchison, and J. K. S. Poon, “Voltage-controlled switching and thermal effects in VO_2 nano-gap junctions”, App. Phys. Lett. **104**(22), 221904 (2014).